PHYSICAL REVIEW D **95,** 094002 (2017)

Transverse single-spin asymmetries in $\ell p^\uparrow \to hX$ within a TMD approach: Role of quasireal photon exchange

Umberto D'Alesio,[1,2,*] Carlo Flore,[1,2,†] and Francesco Murgia[2,‡]

[1]*Dipartimento di Fisica, Università di Cagliari, Cittadella Universitaria, I-09042 Monserrato, Cagliari, Italy*

[2]*INFN, Sezione di Cagliari, Cittadella Universitaria, I-09042 Monserrato, Cagliari, Italy*

(Received 20 February 2017; published 5 May 2017)

We present an updated study of transverse single-spin asymmetries for the inclusive large-P_T processes $\ell p^\uparrow \to hX$ and $\ell p^\uparrow \to \text{jet}X$, within a transverse momentum-dependent approach, including the contribution of quasireal (Weizsäcker-Williams) photons. In the spirit of a unified transverse momentum-dependent scheme, predictions are obtained adopting the Sivers and transversity distributions and the Collins fragmentation functions as extracted from fits to the azimuthal asymmetries measured in semi-inclusive deep inelastic scattering and e^+e^- annihilation processes. The description of the available data is extremely good, showing a clear general improvement with respect to the previous leading-order analysis. Predictions for unpolarized cross sections and single-spin asymmetries for ongoing and future experiments are also given.

DOI: 10.1103/PhysRevD.95.094002

I. INTRODUCTION

The role played by transverse single-spin asymmetries (SSAs) in our understanding of the nucleon structure is nowadays well consolidated and, at the same time, still the source of challenging issues. Indeed, SSAs observed in processes where two energy scales (a large and a small one) are detected are unambiguously studied within an approach based on factorization theorems in terms of transverse momentum-dependent distributions (TMDs). On the other hand, the description of the large data sets for the SSA A_N measured in inclusive pion production in $p^\uparrow p$ collisions, where only one energy scale is present, is still under debate (see for instance Refs. [1,2] for general overviews and Refs. [3–13] for the experimental results).

In Refs. [14,15], this issue was investigated in a somehow theoretically more simple single-inclusive process, $\ell p^\uparrow \to hX$, still characterized by a single large energy scale but very close to the semi-inclusive deep inelastic scattering (SIDIS) process, for which TMD factorization has been proven [16–23].

This process indeed can be considered a sort of bridge between the $p^\uparrow p \to hX$ and $\ell p^\uparrow \to \ell' hX$ processes: it is single inclusive with a single large energy scale (as the $pp \to hX$ process) and at the same time, at leading order, is controlled by the color-blind electromagnetic interaction (as the SIDIS process). This should reduce the role played by initial/final state interactions leading to potential factorization breaking effects. On the other hand, adopting the relevant TMDs (Sivers and Collins functions), as extracted from SIDIS data, in the inclusive hadron production in lepton-proton collisions represents an attempt toward (and a test for) a unified TMD scheme. It is worth mentioning that the same process was also considered in Refs. [24,25] in the framework of collinear factorization with twist-3 correlation functions, while inclusive jet production was studied in Ref. [26].

In Refs. [14,15], to which we refer the reader for all details of the approach, SSAs were computed assuming a TMD factorization scheme at leading order (LO), that is considering only the elementary partonic channel $\ell q \to \ell q$. In particular, in Ref. [15], the theoretical estimates were compared with a selection[1] of the experimental results by the HERMES Collaboration [27], showing good agreement in sign and size. In spite of this, it was also pointed out that some of the discrepancies still present between theory and experiment could be ascribed to effects neglected in a LO treatment.

Here, we want to extend this LO study including the contribution from quasireal photon exchange, in the Weizsäcker-Williams approximation, potentially relevant in the kinematical configuration dominated by small Q^2. This will allow us, still within a TMD scheme, to improve the description of the fully inclusive data and consider, for the first time, the HERMES antitagged data set, dominated by events in which the final lepton (not observed) has a very small scattering angle. Notice that this data category was not included in the previous analysis because a simple LO approach (namely via $\ell q \to \ell q$) is expected to be inadequate.

In this respect, we will benefit from the study performed in Ref. [28], even if with a different perspective and approach. In this work, the authors, within a collinear-factorization

*umberto.dalesio@ca.infn.it
†carlo.flore@ca.infn.it
‡francesco.murgia@ca.infn.it

[1]Only data for inclusive events in the backward target hemisphere at large P_T and tagged events (deep inelastic scattering category) were considered.

scheme, computed the next-to-leading-order (NLO) corrections to the unpolarized cross sections for the same process and discussed the role of quasireal photon exchange. In most kinematical configurations, they found that this contribution represents only a small part of the NLO corrections. They then concluded that only a full NLO treatment could be considered complete.

On the other hand, within a TMD scheme, as well as in the twist-3 approach, NLO corrections are still not available for such a process, and it is then worth seeing to what extent the quasireal photon exchange could play a role in the computation of spin asymmetries. On top of that, and relevant from our point of view, by including transverse momentum effects, the estimates of unpolarized cross sections are enhanced with respect to those computed in a collinear framework. Experimental data, still not available, would definitely help in this respect. Notice that for the process $pp \to \pi X$ the estimates of unpolarized cross sections in a TMD approach at leading order show a reasonable agreement with available data from the Relativistic Heavy Ion Collider (RHIC); see Ref. [29].

The main aim of this study will be then to provide the complete calculation within a TMD formalism of the quasireal photon exchange in $\ell p \to hX$ and $\ell p \to \text{jet}X$ processes and to compute the unpolarized cross sections and the SSAs for various experimental setups.

The paper is organized as follows. In Sec. II, we recall the general formalism, deriving and discussing all new theoretical results. In particular, in Sec. II B, we present, for the first time, the full TMD expressions for the quasireal photon contribution to unpolarized and transversely polarized cross sections for inclusive hadron and inclusive jet production. In Sec. III, we show our phenomenological results, starting with the unpolarized cross sections for HERMES, Jefferson Lab (JLab), COMPASS, and Electron-Ion Collider (EIC) experiments, and then focus on transverse SSAs, with special emphasis on the comparison with HERMES data. Predictions for other experimental setups are also given and discussed. Conclusions and final comments are gathered in Sec. IV.

II. FORMALISM

We consider the transverse single-spin asymmetry, A_N, for the process $p^\uparrow \ell \to hX$ in the proton-lepton center-of-mass frame,

$$A_N = \frac{d\sigma^\uparrow(\boldsymbol{P}_T) - d\sigma^\downarrow(\boldsymbol{P}_T)}{d\sigma^\uparrow(\boldsymbol{P}_T) + d\sigma^\downarrow(\boldsymbol{P}_T)} = \frac{d\sigma^\uparrow(\boldsymbol{P}_T) - d\sigma^\uparrow(-\boldsymbol{P}_T)}{2d\sigma^{\rm unp}(\boldsymbol{P}_T)} = \frac{d\Delta\sigma(\boldsymbol{P}_T)}{2d\sigma^{\rm unp}(\boldsymbol{P}_T)}, \tag{1}$$

where

$$d\sigma^{\uparrow,\downarrow} \equiv \frac{E_h d\sigma^{p^{\uparrow,\downarrow}\ell \to hX}}{d^3\boldsymbol{P}_h} \tag{2}$$

and $\boldsymbol{P}_h$ and $\boldsymbol{P}_T$ are respectively the 3-momentum of the final hadron and its vector transverse component. The polarized proton (or nucleon) is in a pure transverse spin state $\boldsymbol{S}$ and is assumed to move along the positive $Z_{\rm cm}$ axis, while the lepton is taken unpolarized. We define as transverse polarization for the proton the $Y_{\rm cm}$ direction, with $\uparrow$ and $\downarrow$ respectively for protons polarized along or opposite to $Y_{\rm cm}$. The $X_{\rm cm}$ axis is defined in such a way that a hadron h with $(P_h)_{X_{\rm cm}} > 0$ is produced *to the left* of the incoming proton (see also Fig. 1 of Ref. [14]).

Notice that for a generic transverse polarization, $\boldsymbol{S}_T$, along an azimuthal direction ϕ_S in the chosen reference frame, in which the $\uparrow$ direction is given by $\phi_S = \pi/2$, one has

$$A(\phi_S, S_T) = \boldsymbol{S}_T \cdot (\hat{\boldsymbol{p}} \times \hat{\boldsymbol{P}}_T) A_N = S_T \sin\phi_S A_N, \tag{3}$$

where $\boldsymbol{p}$ is the proton momentum. Following the usual definition adopted in SIDIS experiments, one simply obtains

$$A_{TU}^{\sin\phi_S} \equiv \frac{2}{S_T} \frac{\int d\phi_S [d\sigma(\phi_S) - d\sigma(\phi_S + \pi)] \sin\phi_S}{\int d\phi_S [d\sigma(\phi_S) + d\sigma(\phi_S + \pi)]} = A_N. \tag{4}$$

In order to include effects from quasireal photon exchange, adopting the Weizsäcker-Williams (WW) approximation, within a TMD approach, we write the SSA under consideration as follows,

$$A_N = \frac{d\Delta\sigma^{\rm LO} + d\Delta\sigma^{\rm WW}}{2[d\sigma^{\rm LO} + d\sigma^{\rm WW}]}, \tag{5}$$

where the leading-order contributions are given by [14,15],

$$d\Delta\sigma^{\rm LO} = \sum_q \int \frac{dxdz}{16\pi^2 x z^2 s} d^2\boldsymbol{k}_\perp d^3\boldsymbol{p}_\perp \delta(\boldsymbol{p}_\perp \cdot \hat{\boldsymbol{p}}'_q) J(p_\perp) \delta(\hat{s} + \hat{t} + \hat{u}) [\Sigma(\uparrow) - \Sigma(\downarrow)]^{q\ell \to q\ell} \tag{6}$$

$$2d\sigma^{\rm LO} = \sum_q \int \frac{dxdz}{16\pi^2 x z^2 s} d^2\boldsymbol{k}_\perp d^3\boldsymbol{p}_\perp \delta(\boldsymbol{p}_\perp \cdot \hat{\boldsymbol{p}}'_q) J(p_\perp) \delta(\hat{s} + \hat{t} + \hat{u}) [\Sigma(\uparrow) + \Sigma(\downarrow)]^{q\ell \to q\ell}, \tag{7}$$

with $q = u, \bar{u}, d, \bar{d}, s, \bar{s}$ and

$$[\Sigma(\uparrow)-\Sigma(\downarrow)]^{q\ell\to q\ell} = \frac{1}{2}\Delta^N f_{q/p^\uparrow}(x,k_\perp)\cos\phi[|\hat{M}_1^0|^2+|\hat{M}_2^0|^2]D_{h/q}(z,p_\perp) + h_{1q}(x,k_\perp)\hat{M}_1^0\hat{M}_2^0\Delta^N D_{h/q^\uparrow}(z,p_\perp)\cos(\phi'+\phi_q^h) - \frac{k_\perp^2}{2M^2}h_{1T}^{\perp q}(x,k_\perp)\hat{M}_1^0\hat{M}_2^0\Delta^N D_{h/q^\uparrow}(z,p_\perp)\cos(2\phi-\phi'-\phi_q^h) \quad (8)$$

$$[\Sigma(\uparrow)+\Sigma(\downarrow)]^{q\ell\to q\ell} = f_{q/p}(x,k_\perp)[|\hat{M}_1^0|^2+|\hat{M}_2^0|^2]D_{h/q}(z,p_\perp) - \frac{k_\perp}{M}h_1^{\perp q}(x,k_\perp)\hat{M}_1^0\hat{M}_2^0\Delta^N D_{h/q^\uparrow}(z,p_\perp)\cos(\phi-\phi'-\phi_q^h). \quad (9)$$

A proper definition of all functions and variables appearing in the above equations can be found in Ref. [14] and its Appendixes and in Ref. [30]. For a better understanding, we recall here their physical meaning:

(i) $\boldsymbol{k}_\perp = k_\perp(\cos\phi,\sin\phi,0)$ and $\boldsymbol{p}_\perp$ are respectively the transverse momentum of the parton in the proton and of the final hadron with respect to the direction of the fragmenting parent parton, with momentum $\boldsymbol{p}'_q$. Notice that $\boldsymbol{p}$ and $\boldsymbol{p}_\perp$ are different vectors.

(ii) The first term on the rhs of Eq. (8) represents the Sivers effect [31–33], with

$$\Delta\hat{f}_{q/p,S}(x,\boldsymbol{k}_\perp) = \hat{f}_{q/p,S}(x,\boldsymbol{k}_\perp)-\hat{f}_{q/p,-S}(x,\boldsymbol{k}_\perp) \equiv \Delta^N f_{q/p^\uparrow}(x,k_\perp)\,\hat{\boldsymbol{S}}_T\cdot(\hat{\boldsymbol{p}}\times\hat{\boldsymbol{k}}_\perp) = -2\frac{k_\perp}{M}f_{1T}^{\perp q}(x,k_\perp)\,\hat{\boldsymbol{S}}_T\cdot(\hat{\boldsymbol{p}}\times\hat{\boldsymbol{k}}_\perp). \quad (10)$$

The extra factors are the unpolarized elementary interaction [$\propto(|M_1^0|^2+|M_2^0|^2)$] and the unpolarized fragmentation function $D_{h/q}(z,p_\perp)$; in the chosen reference frame, where $\phi_S=\pi/2$, the correlation factor $\hat{\boldsymbol{S}}_T\cdot(\hat{\boldsymbol{p}}\times\hat{\boldsymbol{k}}_\perp)$ gives the modulation $\sin(\phi_S-\phi)=\cos\phi$.

(iii) The second and third terms (this last one numerically negligible) on the rhs of Eq. (8) represent the contribution to A_N of the Collins effect, given respectively as a convolution of the unintegrated transversity distribution, $h_{1q}(x,k_\perp)$, and the pretzelosity distribution, $h_{1T}^{\perp q}(x,k_\perp)$, with the Collins function $\Delta^N D_{h/q^\uparrow}(z,p_\perp)$ [33,34],

$$\Delta\hat{D}_{h/q^\uparrow}(z,\boldsymbol{p}_\perp) = \hat{D}_{h/q^\uparrow}(z,\boldsymbol{p}_\perp)-\hat{D}_{h/q^\downarrow}(z,\boldsymbol{p}_\perp) \equiv \Delta^N D_{h/q^\uparrow}(z,p_\perp)\,\hat{\boldsymbol{s}}_q\cdot(\hat{\boldsymbol{p}}'_q\times\hat{\boldsymbol{p}}_\perp) = \frac{2p_\perp}{zm_h}H_1^{\perp q}(z,p_\perp)\,\hat{\boldsymbol{s}}_q\cdot(\hat{\boldsymbol{p}}'_q\times\hat{\boldsymbol{p}}_\perp). \quad (11)$$

The product $\hat{M}_1^0\hat{M}_2^0$ is related to the spin transfer elementary interaction ($\propto d\hat{\sigma}^{q^\uparrow\ell\to q^\uparrow\ell}-d\hat{\sigma}^{q^\uparrow\ell\to q^\downarrow\ell}$), while the factors $\cos(\phi'+\phi_q^h)$ and $\cos(2\phi-\phi'-\phi_q^h)$ arise from phases in the $\boldsymbol{k}_\perp$-dependent transversity and pretzelosity distributions, the Collins function, and the elementary polarized interaction.

(iv) The first (and dominant) term on the rhs of Eq. (9) is the convolution of the unpolarized TMD parton distribution and fragmentation functions with the unpolarized partonic interactions, while the second one, numerically negligible, represents the Boer-Mulders mechanism [35,36], with the corresponding function defined as

$$\Delta\hat{f}_{q,s/p}(x,\boldsymbol{k}_\perp) = \hat{f}_{q,s/p}(x,\boldsymbol{k}_\perp)-\hat{f}_{q,-s/p}(x,\boldsymbol{k}_\perp) \equiv \Delta^N f_{q^\uparrow/p}(x,k_\perp)\,\hat{\boldsymbol{s}}_T\cdot(\hat{\boldsymbol{p}}\times\hat{\boldsymbol{k}}_\perp) = -\frac{k_\perp}{M}h_1^{\perp q}(x,k_\perp)\,\hat{\boldsymbol{s}}_T\cdot(\hat{\boldsymbol{p}}\times\hat{\boldsymbol{k}}_\perp). \quad (12)$$

In the following sections, we discuss in detail the Weizsäcker-Williams approximation and its role in the (un)polarized process under consideration.

A. Weizsäcker-Williams approximation

As shown in Ref. [28], in a NLO treatment of the inclusive process $\ell p\to hX$, the collinear lepton singularities could be regularized, and opportunely redefined, by introducing a QED parton distribution for the lepton, in strong analogy with the ordinary nucleon's parton distributions. The only difference is that in such a case the partons are the lepton itself and the photon. Without entering into many details, we can say that at order $\alpha^2\alpha_s$ there will be a contribution from the photon acting as a parton of the lepton and entering the hard scattering process. This can be represented as a Weizsäcker-Williams contribution [37,38], where the lepton acts as a source of real photons (see also Refs. [39–41]). We then assume the following factorization formula for the WW contribution to the process $\ell p\to hX$,

$$\sigma^{\rm WW}(\ell p \to hX) = \int dy f_{\gamma/\ell}(y)\sigma(\gamma p \to hX), \qquad (13)$$

where $f_{\gamma/\ell}(y)$ is the number density of photons inside the lepton, carrying a lepton-momentum fraction y ($p_\gamma = y p_\ell$), and $\sigma(\gamma p \to hX)$ is the cross section for the process $\gamma p \to hX$ initiated by a real photon.

For the WW distribution, we follow Ref. [28], adopting

$$f_{\gamma/\ell}(y) = \frac{\alpha}{2\pi}\frac{1+(1-y)^2}{y}\left[\ln\left(\frac{\mu^2}{y^2 m_\ell^2}\right) - 1\right] + \mathcal{O}(\alpha^2), \qquad (14)$$

where α is the electromagnetic coupling constant, μ is the factorization scale, and m_ℓ is the lepton mass. We have also tried an alternative form for the WW distribution, like the one proposed in Refs. [39–41] and adopted, in the context of SSA studies, in Refs. [42,43]. In both cases, we have considered two choices of the factorization scale, namely $\mu = P_T$ or $\mu = \sqrt{s}/2$. Since these choices do not lead to any significant differences, we will present our estimates only for the form in Eq. (14) with $\mu = P_T$.

B. Quasireal photon contribution to SSAs for inclusive particle production

In order to compute the WW contribution to A_N, based on the factorized expression (13), we start with the general treatment for the cross section, in a TMD scheme, of the large-P_T inclusive polarized process $A(S_A)B(S_B) \to CX$ [30], adapted here to the process $p(S)\ell \to hX$,

$$\frac{E_h d\sigma^{p(S)\ell\to hX}_{\rm WW}}{d^3\boldsymbol{P}_h} = \sum_{a,c,d,\{\lambda\}}\int \frac{dxdydz}{16\pi^2 xyz^2 s} d^2\boldsymbol{k}_\perp d^3\boldsymbol{p}_\perp \delta(\boldsymbol{p}_\perp\cdot\hat{\boldsymbol{p}}_c) J(p_\perp)\delta(\hat{s}+\hat{t}+\hat{u}) \times \rho^{a/p,S}_{\lambda_a\lambda_a'}\hat{f}_{a/p,S}(x,\boldsymbol{k}_\perp)\rho^{\gamma/\ell}_{\lambda_\gamma\lambda_\gamma'} f_{\gamma/\ell}(y)\hat{M}_{\lambda_c,\lambda_d;\lambda_a\lambda_\gamma}\hat{M}^*_{\lambda_c',\lambda_d;\lambda_a'\lambda_\gamma'} D^{\lambda_h,\lambda_h}_{\lambda_c,\lambda_c'}(z,\boldsymbol{p}_\perp), \qquad (15)$$

which can be written schematically as

$$d\sigma^{\rm WW}(S) = \sum_{a,c,d}\int \frac{dxdydz}{16\pi^2 xyz^2 s} d^2\boldsymbol{k}_\perp d^3\boldsymbol{p}_\perp \delta(\boldsymbol{p}_\perp\cdot\hat{\boldsymbol{p}}_c) J(p_\perp)\delta(\hat{s}+\hat{t}+\hat{u})\Sigma(S)^{a\gamma\to cd}. \qquad (16)$$

Notice that in Eq. (15) we have consistently adopted a collinear WW distribution, as properly defined for the case of a scattered lepton, and a photon, almost collinear with the initial lepton and that now a, c can be a quark (antiquark) or a gluon (this is at variance with respect to the LO calculation where only quark TMDs are involved).

For the notation and the meaning of the quantities entering Eq. (15), we refer the reader to Refs. [14,30]. Here, we only note that the Mandelstam variables for the process $a\gamma \to cd$ are defined using $p_\gamma = y p_\ell$ and that the ρ's and the $\hat{M}$'s are respectively the helicity density matrices of partons (photons) inside a polarized hadron (an unpolarized lepton) and the helicity amplitudes for the elementary processes $q\gamma \to qg$ and $g\gamma \to q\bar{q}$. We further recall that the $\hat{M}$'s are defined in the proton-lepton c.m. frame, where the $a\gamma \to cd$ processes are not planar. They can be expressed in terms of the corresponding canonical helicity amplitudes $\hat{M}^0$ in the a–γ c.m. frame by performing proper boost and rotations as described in Refs. [30,44] (see also Appendix A).

By summing over the helicities, using the proper definition of the helicity density matrices for spin-1/2 and spin-1 partons and exploiting the parity properties of the helicity amplitudes, we obtain the following expressions for the kernels $\Sigma(S)^{a\gamma\to cd}$:

(1) $q\gamma \to qg$ processes:

$$\Sigma(S) = \frac{1}{2}\hat{f}_{q/p,S}(x,\boldsymbol{k}_\perp) f_{\gamma/\ell}(y)\{D_{h/q}(z,p_\perp)[(|\hat{M}^0_1|^2 + |\hat{M}^0_2|^2) + P^q_z P^\gamma_z(|\hat{M}^0_1|^2 - |\hat{M}^0_2|^2)] - \Delta^N D_{h/q^\uparrow}(z,p_\perp)\hat{M}^0_1\hat{M}^0_2[P^q_x \sin(\varphi_1 - \varphi_2 + \phi^h_q) - P^q_y\cos(\varphi_1 - \varphi_2 + \phi^h_q)]\}, \qquad (17)$$

where q can be either a quark or an antiquark and

$$|\hat{M}^0_1|^2 = -\frac{16}{3}g_s^2 e^2 e_q^2\frac{\hat{s}}{\hat{u}} \qquad |\hat{M}^0_2|^2 = -\frac{16}{3}g_s^2 e^2 e_q^2\frac{\hat{u}}{\hat{s}} \qquad \hat{M}^0_1\hat{M}^0_2 = \frac{16}{3}g_s^2 e^2 e_q^2. \qquad (18)$$

(2) $q\gamma \to gq$ processes:

$$\Sigma(S) = \frac{1}{2}\hat{f}_{q/p,S}(x,\boldsymbol{k}_\perp) f_{\gamma/\ell}(y)\{D_{h/g}(z,p_\perp)[(|\hat{M}_1^0|^2 + |\hat{M}_3^0|^2) + P_z^q P_z^\gamma(|\hat{M}_1^0|^2 - |\hat{M}_3^0|^2)] + \Delta^N D_{h/\mathcal{T}_1^g}(z,p_\perp)\hat{M}_1^0\hat{M}_3^0[\mathcal{T}_1^\gamma \cos(\varphi_1 - \varphi_3 + 2\phi_g^h) + \mathcal{T}_2^\gamma \sin(\varphi_1 - \varphi_3 + 2\phi_g^h)]\}, \tag{19}$$

where again q can be either a quark or an antiquark and

$$|\hat{M}_1^0|^2 = -\frac{16}{3} g_s^2 e^2 e_q^2 \frac{\hat{s}}{\hat{t}} \qquad |\hat{M}_3^0|^2 = -\frac{16}{3} g_s^2 e^2 e_q^2 \frac{\hat{t}}{\hat{s}} \qquad \hat{M}_1^0\hat{M}_3^0 = \frac{16}{3} g_s^2 e^2 e_q^2. \tag{20}$$

(3) $g\gamma \to q\bar{q}$ processes:

$$\Sigma(S) = \frac{1}{2}\hat{f}_{g/p,S}(x,\boldsymbol{k}_\perp) f_{\gamma/\ell}(y) D_{h/q}(z,p_\perp)\{[(1 - P_z^g P_z^\gamma)(|\hat{M}_2^0|^2 + |\hat{M}_3^0|^2)] + 2\hat{M}_2^0\hat{M}_3^0[(\mathcal{T}_1^g\mathcal{T}_1^\gamma + \mathcal{T}_2^g\mathcal{T}_2^\gamma)\cos(\varphi_2 - \varphi_3) + (\mathcal{T}_1^g\mathcal{T}_2^\gamma - \mathcal{T}_2^g\mathcal{T}_1^\gamma)\sin(\varphi_2 - \varphi_3)]\}, \tag{21}$$

where

$$|\hat{M}_2^0|^2 = 2g_s^2 e^2 e_q^2 \frac{\hat{u}}{\hat{t}} \qquad |\hat{M}_3^0|^2 = 2g_s^2 e^2 e_q^2 \frac{\hat{t}}{\hat{u}} \qquad \hat{M}_2^0\hat{M}_3^0 = 2g_s^2 e^2 e_q^2. \tag{22}$$

(4) $g\gamma \to \bar{q}q$ processes:

These can be obtained from the $g\gamma \to q\bar{q}$ processes by interchanging in the above two equations $\hat{t}$ with $\hat{u}$ (that is $\hat{M}_2^0 \leftrightarrow \hat{M}_3^0$ and $\varphi_2 \leftrightarrow \varphi_3$) and $D_{h/q}$ with $D_{h/\bar{q}}$.

In the above equations, $P_i^{q,g,\gamma}$ stand for the quark, gluon, and photon polarization vector components, and $\mathcal{T}_i^{g,\gamma}$ stand for the gluon and photon linear polarization ones, while φ_i are the azimuthal phases of the helicity amplitudes (see Appendix A for details).

We are now ready to compute the WW contributions to A_N. By choosing $\phi_S = \pi/2$ in the adopted reference frame, we have

$$d\Delta\sigma^{\mathrm{WW}} = \sum_{a,c,d}\int \frac{dxdydz}{16\pi^2 xyz^2 s} d^2\boldsymbol{k}_\perp d^3\boldsymbol{p}_\perp \delta(\boldsymbol{p}_\perp \cdot \hat{\boldsymbol{p}}_q')J(p_\perp)\delta(\hat{s} + \hat{t} + \hat{u})[\Sigma(\uparrow) - \Sigma(\downarrow)]^{a\gamma\to cd} \tag{23}$$

$$2d\sigma^{\mathrm{WW}} = \sum_{a,c,d}\int \frac{dxdydz}{16\pi^2 xyz^2 s} d^2\boldsymbol{k}_\perp d^3\boldsymbol{p}_\perp \delta(\boldsymbol{p}_\perp \cdot \hat{\boldsymbol{p}}_q')J(p_\perp)\delta(\hat{s} + \hat{t} + \hat{u})[\Sigma(\uparrow) + \Sigma(\downarrow)]^{a\gamma\to cd}, \tag{24}$$

where

$$\sum_{a,c,d}[\Sigma(\uparrow) \pm \Sigma(\downarrow)]^{a\gamma\to cd} = [\Sigma(\uparrow) \pm \Sigma(\downarrow)]^{q\gamma\to qg} + [\Sigma(\uparrow) \pm \Sigma(\downarrow)]^{q\gamma\to gq} + [\Sigma(\uparrow) \pm \Sigma(\downarrow)]^{\bar{q}\gamma\to\bar{q}g} + [\Sigma(\uparrow) \pm \Sigma(\downarrow)]^{\bar{q}\gamma\to g\bar{q}} + [\Sigma(\uparrow) \pm \Sigma(\downarrow)]^{g\gamma\to q\bar{q}} + [\Sigma(\uparrow) \pm \Sigma(\downarrow)]^{g\gamma\to\bar{q}q}, \tag{25}$$

with

$$[\Sigma(\uparrow) - \Sigma(\downarrow)]^{q\gamma\to qg} = f_{\gamma/\ell}(y)\Big\{\frac{1}{2}\Delta^N f_{q/p^\uparrow}(x,k_\perp)\cos\phi[|\hat{M}_1^0|^2 + |\hat{M}_2^0|^2]^{q\gamma\to qg} D_{h/q}(z,p_\perp) + h_{1q}(x,k_\perp)[\hat{M}_1^0\hat{M}_2^0]^{q\gamma\to qg}\Delta^N D_{h/q^\uparrow}(z,p_\perp)\cos(\phi' + \phi_q^h) - \frac{k_\perp^2}{2M^2} h_{1T}^{\perp q}(x,k_\perp)[\hat{M}_1^0\hat{M}_2^0]^{q\gamma\to qg}\Delta^N D_{h/q^\uparrow}(z,p_\perp)\cos(2\phi - \phi' - \phi_q^h)\Big\} \tag{26}$$

$$[\Sigma(\uparrow)+\Sigma(\downarrow)]^{q\gamma\to qg} = f_{\gamma/\ell}(y) f_{q/p}(x,k_\perp)[|\hat{M}_1^0|^2+|\hat{M}_2^0|^2]^{q\gamma\to qg} D_{h/q}(z,p_\perp) - \frac{k_\perp}{M} h_1^{\perp q}(x,k_\perp)[\hat{M}_1^0\hat{M}_2^0]^{q\gamma\to qg}\Delta^N D_{h/q^\uparrow}(z,p_\perp)\cos(\phi-\phi'-\phi_q^h) \tag{27}$$

$$[\Sigma(\uparrow)-\Sigma(\downarrow)]^{q\gamma\to gq} = \frac{1}{2} f_{\gamma/\ell}(y)\Delta^N f_{q/p^\uparrow}(x,k_\perp)\cos\phi[|\hat{M}_1^0|^2+|\hat{M}_3^0|^2]^{q\gamma\to gq} D_{h/g}(z,p_\perp) \tag{28}$$

$$[\Sigma(\uparrow)+\Sigma(\downarrow)]^{q\gamma\to gq} = f_{\gamma/\ell}(y) f_{q/p}(x,k_\perp)[|\hat{M}_1^0|^2+|\hat{M}_3^0|^2]^{q\gamma\to gq} D_{h/g}(z,p_\perp) \tag{29}$$

$$[\Sigma(\uparrow)-\Sigma(\downarrow)]^{g\gamma\to q\bar{q}} = \frac{1}{2} f_{\gamma/\ell}(y)\Delta^N f_{g/p^\uparrow}(x,k_\perp)\cos\phi[|\hat{M}_2^0|^2+|\hat{M}_3^0|^2]^{g\gamma\to q\bar{q}} D_{h/q}(z,p_\perp) \tag{30}$$

$$[\Sigma(\uparrow)+\Sigma(\downarrow)]^{g\gamma\to q\bar{q}} = f_{\gamma/\ell}(y) f_{g/p}(x,k_\perp)[|\hat{M}_2^0|^2+|\hat{M}_3^0|^2]^{g\gamma\to q\bar{q}} D_{h/q}(z,p_\perp), \tag{31}$$

and once again in Eqs. (26)–(29), q can be either a quark or an antiquark, while for the $g\gamma\to\bar{q}q$ channel, one can use the last two relations replacing $D_{h/q}$ with $D_{h/\bar{q}}$. In Eqs. (26) and (27), we have redefined $\varphi_1-\varphi_2=\phi'-\phi$, consistently, and in agreement, with the notation adopted in the LO expressions.[2]

In Eqs. (26) and (28), we recognize the Sivers and Collins effects. Once again, as for the LO piece, the terms involving the pretzelosity in Eq. (26) and the Boer-Mulders function in Eq. (27) are numerically negligible (even saturating their positivity bounds). On the other hand, at variance with the leading-order analysis, we have also a potential contribution from the gluon Sivers function [see Eq. (30)]. Notice that all contributions from linearly polarized gluons ($\mathcal{T}^g$) appearing in Eq. (21) disappear since they are coupled to linearly polarized photon ($\mathcal{T}^\gamma$) distributions that are identically zero for an unpolarized initial lepton.

1. SSAs in single-inclusive jet production at large transverse momentum

Inclusive jet production in lepton-proton collisions, although more difficult to measure, could be an invaluable tool to access the Sivers effect, as the lack of any fragmentation process forbids other contributions. In Ref. [14], this case was discussed, and some results for a high-energy electron-nucleon collider were presented. In the same spirit, here, we extend this analysis including the quasireal photon contribution. The expressions can be directly obtained from the case of inclusive hadron production by replacing the fragmentation functions with proper Dirac delta functions. We report here the main results for the WW contribution, referring to Ref. [14] for the LO piece. For the master formula, we have

$$\frac{E_j d\sigma_{\rm WW}^{(p,S)\ell\to {\rm jet}X}}{d^3\boldsymbol{P}_j} = \sum_{a,c,d,\{\lambda\}}\int\frac{dxdy}{16\pi^2 xys} d^2\boldsymbol{k}_\perp\delta(\hat{s}+\hat{t}+\hat{u}) \times \rho^{a/p,S}_{\lambda_a\lambda_a'}\hat{f}_{a/p,S}(x,\boldsymbol{k}_\perp)\rho^{\gamma/\ell}_{\lambda_\gamma\lambda_\gamma'} f_{\gamma/\ell}(y) \times \hat{M}_{\lambda_c,\lambda_d;\lambda_a\lambda_\gamma}\hat{M}^*_{\lambda_c,\lambda_d;\lambda_a'\lambda_\gamma'}, \tag{32}$$

while for the contributions to $A_N({\rm jet})$,

$$d\Delta\sigma_{\rm jet}^{\rm WW} = \sum_{a,c,d}\int\frac{dxdy}{16\pi^2 xys} d^2\boldsymbol{k}_\perp\delta(\hat{s}+\hat{t}+\hat{u}) \times [\Sigma(\uparrow)-\Sigma(\downarrow)]^{a\gamma\to cd}_{\rm jet} \tag{33}$$

$$2d\sigma_{\rm jet}^{\rm WW} = \sum_{a,c,d}\int\frac{dxdy}{16\pi^2 xys} d^2\boldsymbol{k}_\perp\delta(\hat{s}+\hat{t}+\hat{u}) \times [\Sigma(\uparrow)+\Sigma(\downarrow)]^{a\gamma\to cd}_{\rm jet}, \tag{34}$$

with Eq. (25) still valid also for jet production. For the sums and differences of the kernels, we can use the same expressions as given in Eqs. (26)–(31) replacing $D_{h/q,g}(z,p_\perp)$ with 1 and $\Delta^N D_{h/q^\uparrow}(z,p_\perp)$ with 0. In this case, obviously, there is no fragmentation process, and only the Sivers effect contributes to A_N. Notice that in the present treatment the jet coincides with a single final parton.

III. PHENOMENOLOGICAL RESULTS, COMPARISON WITH DATA, AND PREDICTIONS

In this section, we present our theoretical estimates of the unpolarized cross sections and the SSAs for inclusive pion production in lepton-proton collisions, focusing on the role of the WW contribution and its relevance with respect to the LO approximation. In particular, we will discuss in some detail HERMES kinematics, for which transverse SSA data are available. We will then give predictions for experiments

[2]Notice that the explicit calculation of the azimuthal phases given in Ref. [14] leads to the same results obtained following the boost-rotation procedure described in Refs. [30,44].

at JLab with the upgrade at 12 GeV, for COMPASS at CERN, and for a future electron-ion collider. In this last case, we will also show some estimates for inclusive jet production.

Before presenting our results, it is worth giving some comments on the adopted kinematical configuration with respect to usual experimental setups.

According to the HERMES analysis [27], for instance, the lepton is assumed to move along the positive $Z_{\rm cm}$ axis, so we should consider the processes $\ell p^\uparrow \to hX$, rather than $p^\uparrow \ell \to hX$. In this reference frame, the $\uparrow$ ($\downarrow$) direction is still along the $+Y_{\rm cm}$ ($-Y_{\rm cm}$) axis and, keeping the usual definition of $x_F = 2P_L/\sqrt{s}$, where P_L is the longitudinal momentum of the final hadron, only the sign of x_F is reversed.

The azimuthal-dependent cross section measured by HERMES is defined as [27]

$$d\sigma = d\sigma_{UU}[1 + S_T A_{UT}^{\sin\psi} \sin\psi], \tag{35}$$

where

$$\sin\psi = \hat{\boldsymbol{S}}_T \cdot (\hat{\boldsymbol{P}}_T \times \hat{\boldsymbol{k}}) \tag{36}$$

coincides with our $\sin\phi_S$ of Eq. (3), as $\boldsymbol{p}$ and $\boldsymbol{k}$ (respectively the proton and the lepton 3-momenta) are opposite vectors in the lepton-proton c.m. frame and one has

$$A_{UT}^{\sin\psi}(x_F, P_T) = A_N^{p^\uparrow \ell \to hX}(-x_F, P_T), \tag{37}$$

where $A_N^{p^\uparrow \ell \to hX}$ is the SSA that we compute here and $A_{UT}^{\sin\psi}$ is the quantity measured by HERMES [27].

In the following, to keep uniform the presentation of our results, we will show our predictions adopting the HERMES setup also for JLab and COMPASS experiments. For the EIC, we prefer to keep the other configuration, with the proton moving along the positive $Z_{\rm cm}$ axis, since it allows us to emphasize the strong analogies with the SSAs observed in $p^\uparrow p \to hX$ processes.

Finally, we notice that at relatively low P_T, around 1–2 GeV, due to the inclusion of transverse momentum effects, one or more of the partonic Mandelstam variables might become smaller than a typical hadronic scale. This configuration would correspond to a situation where the propagator of the exchanged particle in the partonic scattering becomes soft. In order to avoid such a potential problem, following Ref. [45], we have introduced an infrared regulator mass ($\mu_0 = 0.8$ GeV). We have checked that shifting the partonic Mandelstam invariants by this quantity squared or cutting them out below it gives similar results. Estimates will be shown adopting the shifting procedure.

A. Unpolarized cross sections

For the computation of the unpolarized cross sections within the adopted TMD approach, we will use the following factorized expressions for the unpolarized TMDs,

$$f_{a/p}(x, k_\perp) = f_{a/p}(x) \frac{1}{\pi \langle k_\perp^2 \rangle} e^{-k_\perp^2/\langle k_\perp^2 \rangle}$$
$$D_{h/c}(z, p_\perp) = D_{h/c}(z) \frac{1}{\pi \langle p_\perp^2 \rangle} e^{-p_\perp^2/\langle p_\perp^2 \rangle}, \tag{38}$$

with $\langle k_\perp^2 \rangle = 0.25$ GeV^2 and $\langle p_\perp^2 \rangle = 0.2$ GeV^2 as extracted in Ref. [46]. For the collinear parton distributions, $f_{a/p}(x)$, we adopt the GRV98 set [47], while for the collinear fragmentation functions (FFs), $D_{h/c}(z)$, we use the Kretzer set [48] and the one by de Florian, Sassot and Stratmann (DSS) [49]. The reasons for this choice are the following: these sets were adopted in the extraction of the Sivers and Collins functions we use here for the calculation of the SSAs (next section); they are characterized by a different role of the gluon fragmentation function, that could play a role in the WW contribution.

1. HERMES

In Figs. 1 and 2, we present our estimates for the unpolarized cross sections for π^+ (left panels) and π^- (right panels) production at $\sqrt{s} \simeq 7.25$ GeV respectively at fixed $x_F = 0.2$ as a function of P_T and at fixed $P_T = 1.4$ GeV as a function of x_F. The thin curves refer to the LO calculation, while the thick ones refer to the total (LO + WW) contribution. In particular, the blue dashed lines are obtained by adopting the Kretzer set for the fragmentation functions, while the red solid lines are obtained with the DSS set.

We start noticing that at LO there are almost no differences between the estimates based on the two FF sets, while these become more significant when also the WW piece is included. The reason is due to the much larger gluon fragmentation function in the DSS set with respect to the Kretzer one, that enters through the $\gamma q \to gq$ process. More interesting from our point of view are the following features: from Fig. 1, we see that the WW piece plays a more relevant role at smaller P_T, being almost three times bigger than the LO term around $P_T = 1$ GeV. This can be ascribed to the smaller values of y reached at low P_T and the corresponding enhancing factor coming from the WW distribution [see Eq. (14)]. Moreover, as one can see in Fig. 2, its contribution is strongly asymmetric in x_F (more than the LO term), being more important for (large) positive x_F values of the final hadron. This could appear surprising, since in such a configuration the lepton undergoes, on average, a backward scattering, and one would expect a lesser role from quasireal photon exchange. On the other hand, for large positive x_F, when the final hadron (as well as its parent parton c) is produced in the *backward* proton hemisphere, $|\hat{u}| \ll |\hat{t}|$, where $\hat{t} = (p_a - p_c)^2$ and $\hat{u} = (p_\gamma - p_c)^2$ for the $a\gamma \to cd$ process. This is the region favored by the

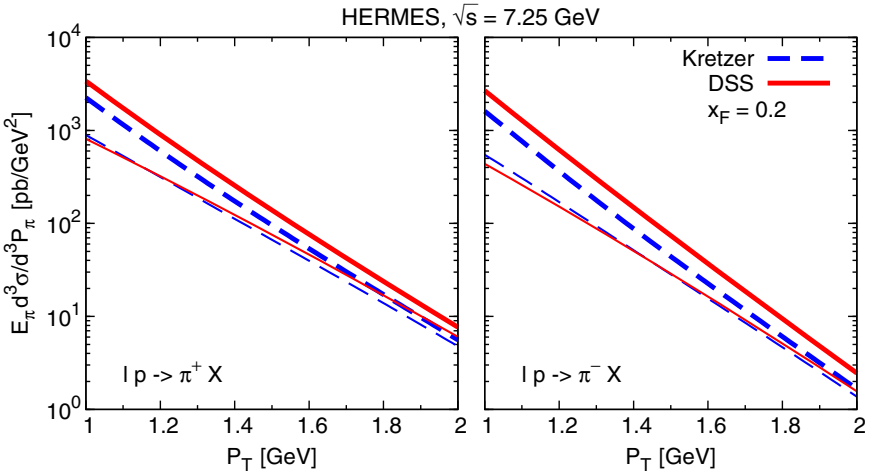

FIG. 1. Estimates of the unpolarized cross sections at $x_F = 0.2$ as a function of P_T for π^+ (left panel) and π^- (right panel) production in $\ell p \to \pi X$, at HERMES, $\sqrt{s} = 7.25$ GeV, adopting two sets for the fragmentation functions: Kretzer set (blue dashed lines) and DSS set (red solid lines). The thin curves represent the LO calculation, while the thick curves represent the total (LO + WW) result.

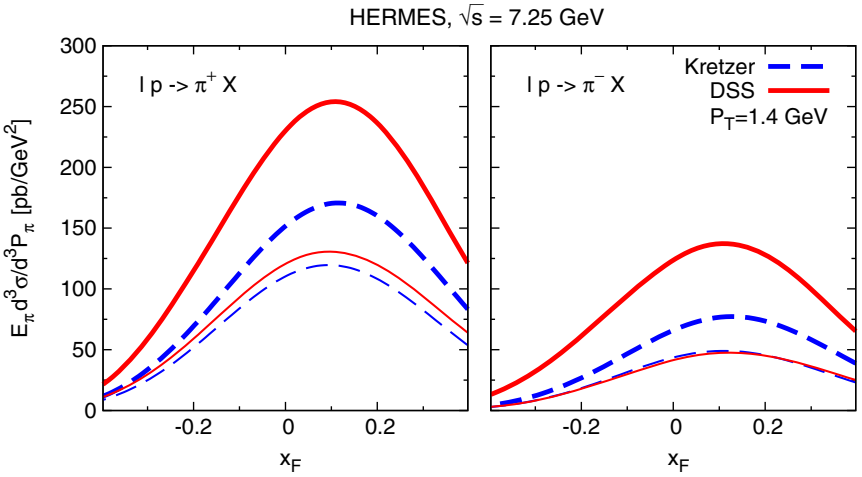

FIG. 2. Estimates of the unpolarized cross sections at $P_T = 1.4$ GeV as a function of x_F for π^+ (left panel) and π^- (right panel) production in $\ell p \to \pi X$, at HERMES, $\sqrt{s} = 7.25$ GeV. Curves have the same meaning as in Fig. 1.

WW contribution with respect to the LO piece since this one goes like $1/Q^2 \equiv 1/\hat{t}^2$, while the partonic cross section for the dominant subprocess $q\gamma \to qg$ [see Eqs. (27) and (18)] goes like $1/\hat{s}\,\hat{u}$.

2. Jefferson Lab at 12 GeV

We consider the process $\ell^3\mathrm{He} \to \pi X$ and, adopting $SU(2)$ symmetry, give estimates at $\sqrt{s} = 4.84$ GeV for the cross section *per nucleon*. In particular, we plot

$$\frac{d^2\sigma}{dx_F dP_T} = \frac{2\pi P_T}{\sqrt{x_F^2 + x_T^2}} E_\pi \frac{d^3\sigma}{d^3\boldsymbol{P}_\pi}, \tag{39}$$

where $x_T = 2P_T/\sqrt{s}$.

In Figs. 3 and 4, we present the unpolarized cross sections for π^+ (left panels) and π^- (right panels) production at $\sqrt{s} \simeq 4.84$ GeV respectively at fixed $x_F = 0.2$ as a function of P_T and at fixed $P_T = 1.5$ GeV as a function of x_F. The curves have the same meaning as for the HERMES kinematics. Same considerations are also valid, with the only extra remark, see Fig. 4, that even the LO calculation gives sizeably different results adopting the two FF sets. This is due to the more important role of the DSS FFs in the very large-z region, as explored at this energy.

3. COMPASS

For the COMPASS experiment, the incoming lepton is a muon with a lab energy of 160 GeV, resulting in $\sqrt{s} = 17.4$ GeV. Following their setup, we use the c.m. pseudorapidity η of the produced hadron in the range $-0.1 < \eta < 2$ (as covered by the COMPASS spectrometer). Similarly to the HERMES configuration, pseudorapidity is counted as

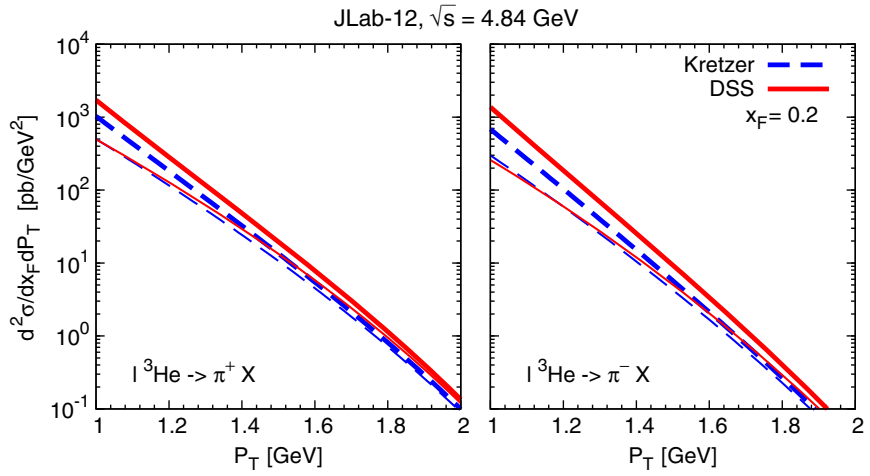

FIG. 3. Estimates of the unpolarized cross sections per nucleon at $x_F = 0.2$ as a function of P_T for π^+ (left panel) and π^- (right panel) production in $\ell^3\mathrm{He} \to \pi X$, at JLab-12, $\sqrt{s} = 4.84$ GeV. Curves have the same meaning as in the previous figures.

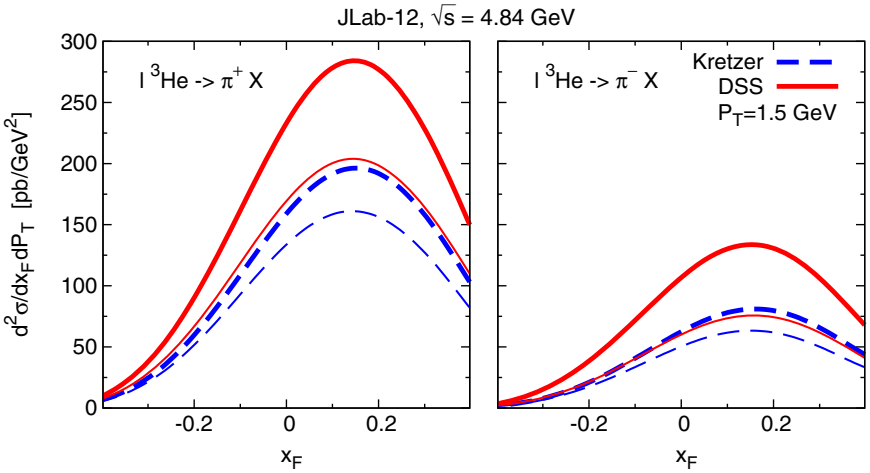

FIG. 4. Estimates of the unpolarized cross sections per nucleon at $P_T = 1.5$ GeV as a function of x_F for π^+ (left panel) and π^- (right panel) production in $\ell^3\mathrm{He} \to \pi X$, at JLab-12, $\sqrt{s} = 4.84$ GeV. Curves have the same meaning as in the previous figures.

positive in the forward direction of the incident muon. We have

$$\frac{d^2\sigma}{d\eta dP_T} = 2\pi P_T E_\pi \frac{d^3\sigma}{d^3\boldsymbol{P}_\pi}. \tag{40}$$

In Fig. 5, we show the unpolarized cross sections for π^+ (left panel) and π^- (right panel) production at $\sqrt{s} = 17.4$ GeV and fixed $P_T = 2$ GeV as a function of η. The curves have the same meaning as in the previous figures. In this case, the two FF sets give almost the same LO results. At variance with what happens for the HERMES configuration, here the WW contribution, although still relevant, plays a lesser role: adopting the DSS set, for instance, it is at most 65% of the LO term for π^- and only 30% for π^+ production. Indeed, the muon mass is almost 200 times bigger than the electron mass, thus reducing the size of the logarithmic piece entering Eq. (14), partially cancelled by the finite term.

4. Electron-ion collider

The proposed future EIC with $\sqrt{s} = 100$ GeV [50] will allow us to study the cross section for single-inclusive pion production in electron-proton collisions at very high energies, comparable to those reached in proton-proton reactions. In such a case, we prefer to adopt the configuration in which the proton moves along the positive Z_{cm} axis, defining x_F accordingly (more precisely, $x_F > 0$ here will refer to the *forward* proton hemisphere). This choice will appear more natural and helpful in the context of the analysis of transverse single-spin asymmetries (next section), allowing an easier comparison with A_N measured in pp collisions. For the same reason, we will consider neutral pion production.

In Fig. 6, we show the unpolarized cross sections for π^0 production at $\sqrt{s} = 100$ GeV respectively at fixed $P_T = 2$ GeV as a function of x_F (left panel) and at fixed $x_F = 0.2$ as a function of P_T (right panel). The curves have the same meaning as in the previous figures. Once again, the two FF

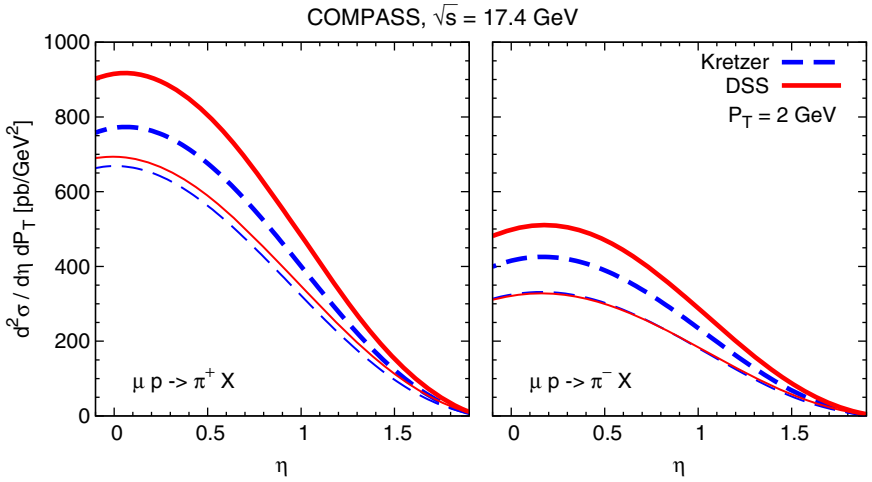

FIG. 5. Estimates of the unpolarized cross sections at $P_T = 2$ GeV as a function of η for π^+ (left panel) and π^- (right panel) production in $\mu p \to \pi X$, at COMPASS, $\sqrt{s} = 17.4$ GeV. Curves have the same meaning as in the previous figures.

sets give almost the same LO results. At variance with what happens at lower energies, here the WW contribution turns out to be much more relevant, being up to four times larger than the LO term at $P_T = 2$ GeV. The reason is that at such large energies and not so large P_T, for $x_F \geq 0$, we probe the small-y region of the photon spectrum in the WW distribution, that behaves like $1/y$, while for $x_F < 0$ (the backward region here), the WW partonic cross sections dominate the LO one, since $|\hat{u}| \ll |\hat{t}|$.

At the EIC, given the large energy available, the interesting study of inclusive jet production could be feasible. In Fig. 7, we give some estimates of the cross sections for jet production at fixed $P_{jT} = 2.5$ GeV as a function of $x_F = 2P_{jL}/\sqrt{s}$ (left panel) and at fixed $x_F = 0.2$ as a function of P_{jT} (right panel). The slightly larger P_{jT} value considered helps keep potential infrared divergences in the hard elementary scattering under better control. Even here, the WW contribution heavily dominates the LO term over almost the full x_F range (with its characteristic asymmetric behavior). Notice that in this case both at large positive and large negative x_F there is no dilution from the large-z behavior of fragmentation functions as happens in inclusive pion production.

B. Transverse single-spin asymmetries

We now focus on the main issue of this paper, the study of the role of quasireal photon exchange in SSAs for single-inclusive particle production in lepton-proton collisions, starting with a comparison with the available data from the HERMES Collaboration [27]. In our computations, based on a TMD factorization scheme, we consider two different sets of the quark Sivers and Collins functions (the latter coupled to the transversity distribution), as previously obtained in a series of papers from fits of SIDIS and e^+e^- data [51–54].

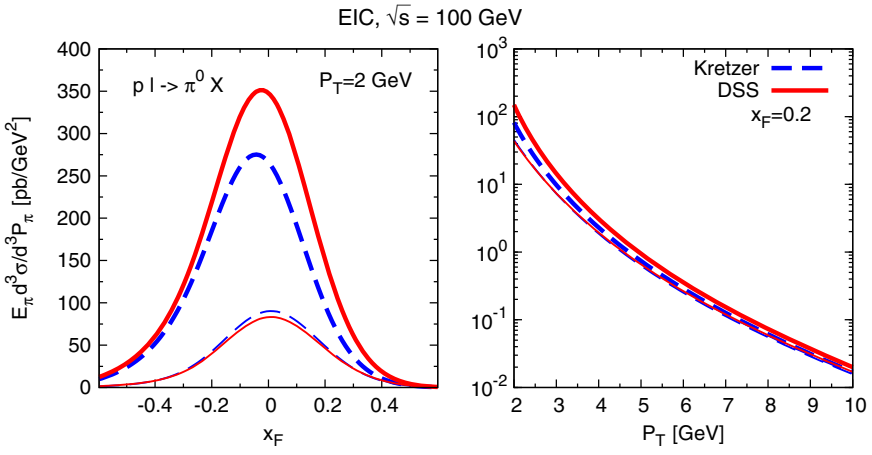

FIG. 6. Estimates of the unpolarized cross sections in $p\ell \to \pi^0 X$, at the EIC, $\sqrt{s} = 100$ GeV, at $P_T = 2$ GeV as a function of x_F (left panel) and at fixed $x_F = 0.2$ as a function of P_T (right panel). Notice that $x_F > 0$ here corresponds to the forward proton hemisphere. Curves have the same meaning as in the previous figures.

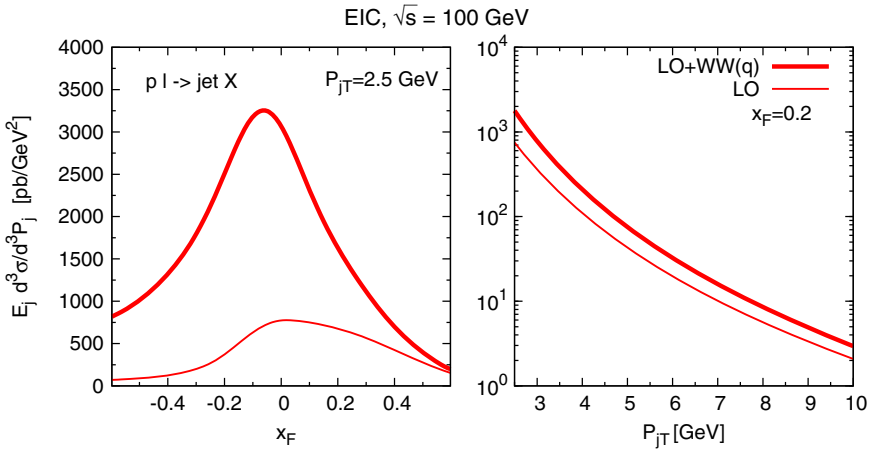

FIG. 7. Estimates of the unpolarized cross sections in $p\ell \to \text{jet}X$, at the EIC, $\sqrt{s} = 100$ GeV at $P_{jT} = 2.5$ GeV as a function of x_F (left panel) and at $x_F = 0.2$ as a function of P_{jT} (right panel). Notice that $x_F > 0$ here corresponds to the forward proton hemisphere. Thick (thin) curves refer to the LO + WW (LO) contribution.

These sets, besides some differences in the initial assumptions and in the data used for their extraction, differ in the choice of the collinear fragmentation functions. More precisely, for the fits [51,52] (SIDIS 1), the Kretzer FF set was adopted, while for the fits [53,54] (SIDIS 2), the DSS FF set was employed. The SIDIS 1 and SIDIS 2 sets are well representative of the extractions of these TMDs and their uncertainties. Concerning the gluon Sivers function, still poorly determined, we adopt the recent extractions of Ref. [55]. Notice that these are obtained assuming a specific set for the quark Sivers functions, and therefore we will have a gluon Sivers function associated to each SIDIS set. It is worth recalling that the extractions of the quark and gluon Sivers functions (as well of the transversity distribution) are constrained only up to $x \simeq 0.3$.

In the following, we will consider both the fully inclusive HERMES data, already discussed in Ref. [15], as well as the subsample of antitagged data (with no detection of the final lepton), for $\ell p^{\uparrow} \to \pi X$ processes at large P_T. In both cases, there is only one large scale (needed for a perturbative calculation), the P_T of the final pion. For this reason, we only look at those data at $P_T \geq 1$ GeV.

At variance with SIDIS azimuthal asymmetries, where the single contributions to A_N coming from the Sivers and Collins effects can be accessed separately by looking at their proper azimuthal modulations, here the two effects could contribute together and mix up. For this reason, we will present for each SIDIS set the overall contribution, adding together the quark Sivers (dominant) and Collins (almost negligible) effects. This will be done for the LO and the complete (LO + WW) calculation. For this last one, we will also show the overall statistical uncertainty bands given as the envelope of the uncertainties on the quark Sivers and Collins functions, obtained following the procedure described in Appendix A of Ref. [53]. For completeness, but with a word of caution, we have also computed the results obtained adding the contribution from the gluon Sivers function. In the following, we will show them explicitly only for HERMES kinematics.

1. HERMES: SSAs and comparison with data

Our predictions for $A_{UT}^{\sin\psi}$, for inclusive π^+ (upper panels) and π^- (lower panels) production, as a function of x_F at $P_T = 1.1$ GeV, compared with the fully inclusive HERMES data [27], are presented in Fig. 8 (this is the only bin at relatively large P_T). More precisely, we show the LO calculation, blue dashed lines, and the complete result adding the WW piece, red solid lines, adopting the quark Sivers and Collins functions from the SIDIS 1 (left panels) and SIDIS 2 (right panels) sets. The overall statistical uncertainty band is also shown. The green dot-dashed lines represent the total contribution including also the gluon Sivers effect.

We can then make the following remarks: the inclusion of the WW contribution (that in this kinematical region dominates the unpolarized cross sections) improves significantly the agreement with the data; the Collins effect is always tiny or completely negligible (both in the LO and WW contributions); the differences between the predictions adopting the SIDIS 1 and SIDIS 2 sets are due to the different behavior of the corresponding Sivers functions; the contribution coming from the gluon Sivers function is almost negligible for the SIDIS 2 set, while that for the SIDIS 1 set is relatively more important, reducing the agreement with the data. We have nevertheless to point out that there is still a large uncertainty in the gluon Sivers function extraction in the large-x region, as covered in such a kinematical configuration.

In Fig. 9, we present, for the first time, our results for the antitagged category for $A_{UT}^{\sin\psi}$, compared with HERMES data [27], at fixed $x_F = 0.2$ (average value of the data set)

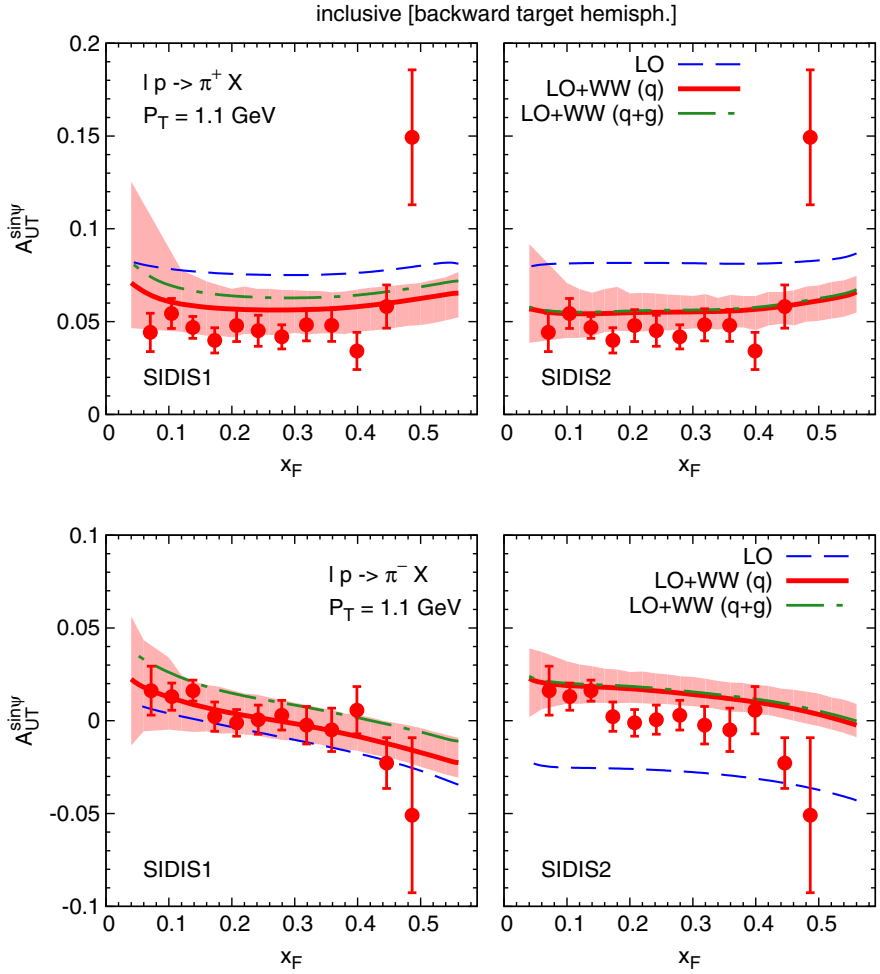

FIG. 8. Theoretical estimates for $A_{UT}^{\sin\psi}$ vs x_F at $\sqrt{s} \simeq 7.25$ GeV and $P_T = 1.1$ GeV for inclusive π^+ (upper panels) and π^- (lower panels) production in $\ell p^\uparrow \to \pi X$ processes, compared with the fully inclusive HERMES data [27]. Two sets for the Sivers and Collins functions have been considered: the SIDIS 1 set (left panels) and the SIDIS 2 set (right panels). More precisely, we show both the LO (blue dashed lines) and LO + WW (red solid lines) quark contributions, as well as the total result including the gluon Sivers effect (green dot-dashed lines). The overall statistical uncertainty band, obtained following the procedure described in Appendix A of Ref. [53] is also shown.

as a function of P_T. Once again, we consider the inclusive π^+ (upper panels) and π^- (lower panels) production, adopting two sets for the quark Sivers and Collins functions: SIDIS 1 (left panels) and SIDIS 2 (right panels). The curves have the same meaning as for the fully inclusive case. From these results, we can observe that once again the WW contribution leads to a much better description of the data (even if some sizeable discrepancy for the π^+ data remains). The gluon Sivers effect is negligible, except for the SIDIS 1 set in π^- production. However, this kinematical region probes the still poorly constrained large-x behavior of the Sivers functions (the dominant contribution), which reflects into wider statistical error bands.

2. SSAs at JLab

Forthcoming measurements at the energy of 12 GeV are going to be performed at JLab (the 6 GeV energy setup is not able to provide sufficiently large-P_T values), on transversely polarized proton, neutron, and deuteron targets. We focus here, for its complementarity with HERMES data, on the neutron target. Indeed, the combined analysis of proton and neutron target events will help in our understanding of the flavor decomposition and on the role of the up and down quark contributions.

Our estimates for the JLab SSAs, $A_{UT}^{\sin\phi_S}$, for inclusive pion production off the polarized ^{3}He (neutron) target are shown in Fig. 10 at fixed $P_T = 1.5$ GeV as a function of x_F. Notice that this somehow large-P_T value has been chosen for uniformity with what was discussed for the unpolarized cross section and because it allows us to span a larger region in x_F (in particular its positive values). We recall that we keep adopting the HERMES configuration, with the incoming lepton moving along the positive $Z_{\rm cm}$ axis, and plot $A_{UT}^{\sin\phi_S} \equiv A_{UT}^{\sin\psi}$. In particular, we show for the

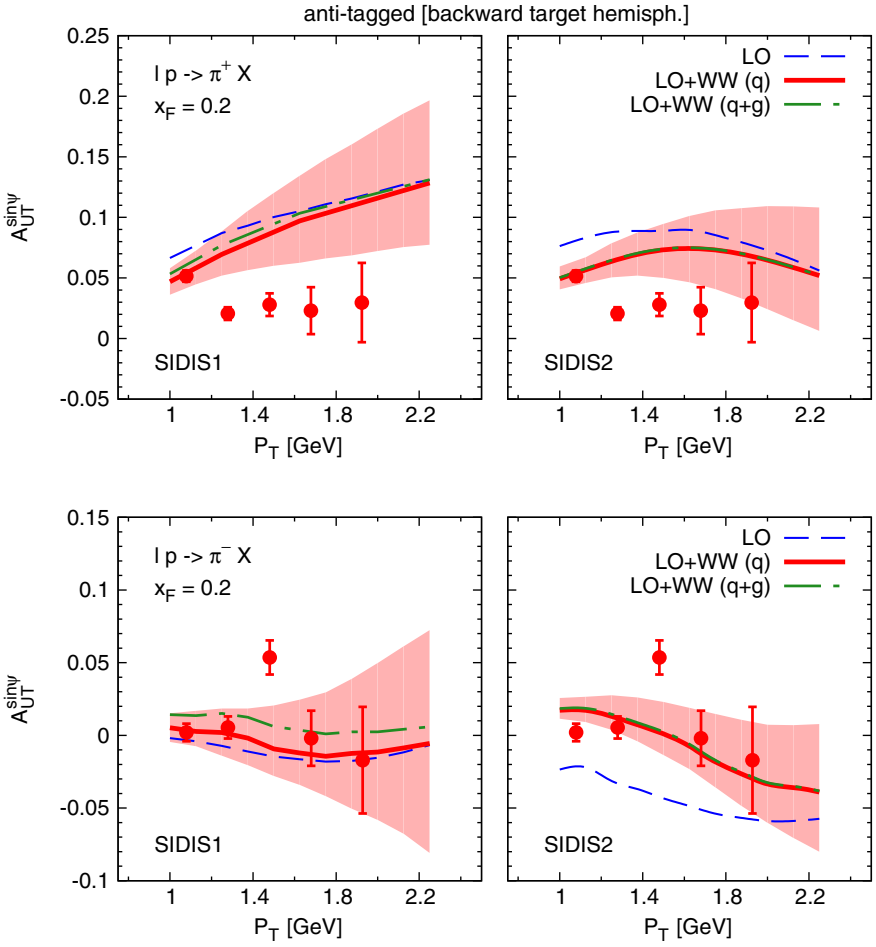

FIG. 9. Theoretical estimates for $A_{UT}^{\sin\psi}$ vs P_T at $\sqrt{s} \simeq 7.25$ GeV and $x_F = 0.2$ for inclusive π^+ (upper panels) and π^- (lower panels) production in $\ell p^\uparrow \to \pi X$ processes, compared with the antitagged HERMES data [27]. Curves have the same meaning as in the previous figure.

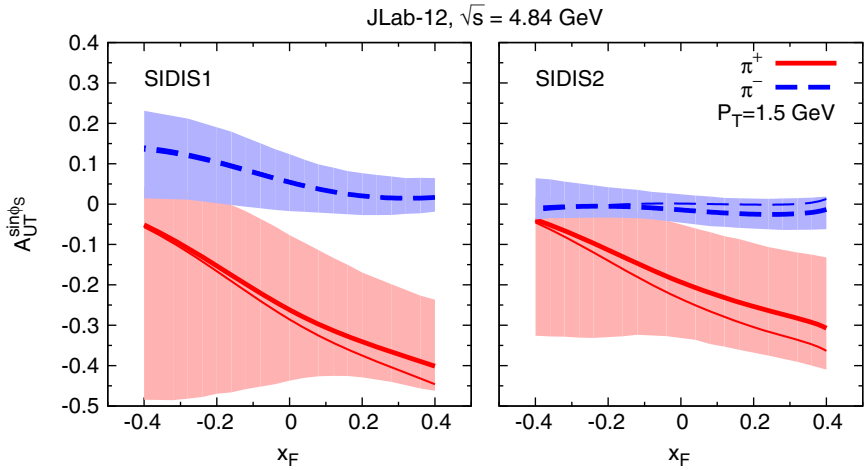

FIG. 10. Theoretical estimates for $A_{UT}^{\sin\phi_S}$ vs x_F at $\sqrt{s} \simeq 4.84$ GeV and $P_T = 1.5$ GeV for inclusive π^+ (red solid lines) and π^- (blue dashed lines) production, which will be measured at JLab operating on a polarized ^{3}He (neutron) target, with a beam energy of 12 GeV. The thin curves refer to the LO calculation, while the thick ones refer to the full, LO + WW, estimates for the two sets for the quark Sivers and Collins functions: SIDIS 1 (left panel) and SIDIS 2 (right panel). The overall statistical uncertainty band, obtained following the procedure described in Appendix A of Ref. [53], is also shown.

SIDIS 1 (left panel) and the SIDIS 2 (right panel) the LO (thin lines) and the LO + WW (thick lines) calculation, displaying also the uncertainty bands for the total contribution. The gluon Sivers effect, not included, plays some role only in π^- production when adopting the SIDIS 1 set, as in the HERMES case, being otherwise negligible. In most cases, the full, LO + WW, estimates present the same behavior, in size and sign, as the LO ones. Nevertheless, one has to keep in mind that, with the DSS FF set for instance, the WW piece alone is about 50% (90%) of the LO contribution for π^+ (π^-) production in this kinematical region. The wider uncertainty bands are due to the large-x region probed at such moderate energies, where the current extractions of the Sivers functions are still unconstrained.

It is worth noticing that the differences with respect to the corresponding HERMES results are due to the exchanged role of the up and down quark Sivers distributions when adopting SU(2) symmetry for a neutron target (JLab). This reflects also in the relative weight of the WW piece when going from positively to negatively charged pions. Moreover, the very large size of A_N for π^+ production at large positive x_F (backward neutron hemisphere), both adopting the SIDIS 1 and the SIDIS 2 sets, is due to the probed values of the quark light-cone momentum fraction in the polarized neutron (down to 0.1 at $x_F > 0$). For such x values, the negative up quark neutron Sivers function (down quark for a proton) is quite large for these two sets and, coupling to the favored fragmentation function, largely dominates over the other contributions.

3. SSAs at COMPASS

Another place where these SSAs could be measured is certainly the COMPASS experiment. Here, we present some estimates for this experimental setup. In Fig. 11, we show $A_{UT}^{\sin\phi_S}$ vs x_F at $\sqrt{s} \simeq 17.4$ GeV and $P_T = 2$ GeV for inclusive π^+ (red solid lines) and π^- (blue dashed lines) production in $\mu p^\uparrow \to \pi X$. Curves have the same meaning as in the previous figures. One can see that the SSAs for π^+ production are expected to be sizeable, with quite narrow error bands; a clear test of this approach could be then carried out. Again, the inclusion of the WW contribution changes only slightly the LO estimates.

4. SSAs at EIC

In Refs. [14,15], some estimates for inclusive jet and inclusive neutral pion production for an electron-nucleon collider at 50 GeV were given with the aim of checking whether some features of the SSAs observed in $p^\uparrow p \to \pi X$, and reproduced in a TMD scheme, could be also encountered in the process under consideration. In such a case, it is more convenient to adopt the configuration where the polarized proton is moving along the positive $Z_{\rm cm}$ axis and positive x_F values correspond to the forward proton hemisphere.

It is then interesting to see what happens when one includes also the contribution from quasireal photon exchange at the future EIC.

In Fig. 12, we show our estimates at $\sqrt{s} = 100$ GeV for $A_{TU}^{\sin\phi_S} \equiv A_N$ [as defined in Eq. (4)] for inclusive π^0 production in $p^\uparrow \ell \to \pi X$ vs x_F at $P_T = 2$ GeV (left panel) and for inclusive jet production vs P_{jT} at $x_F = 0.2$ (right panel), adopting the SIDIS 1 set. This set indeed is the one that better reproduces the behavior of A_N in $p^\uparrow p \to \pi X$ processes (see for instance Ref. [29]) and that is consistent with the findings of a dedicated study performed in Ref. [56]. Again, thick (thin) curves represent LO + WW (LO) contributions. Some comments are in order:

(i) The gluon Sivers effect (not shown) is completely negligible.

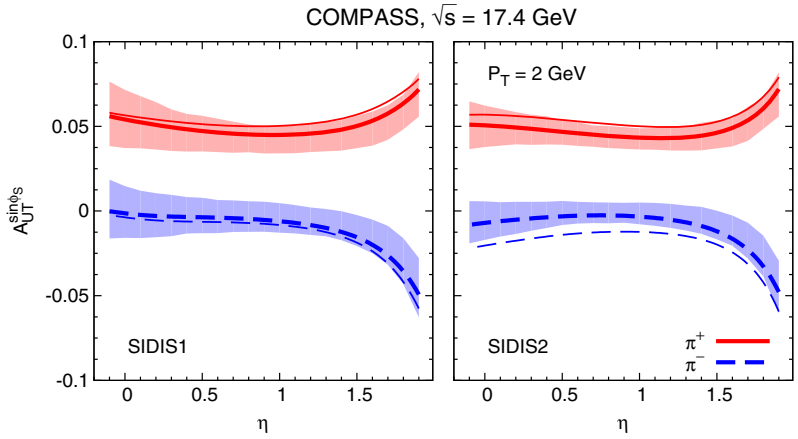

FIG. 11. Theoretical estimates for $A_{UT}^{\sin\phi_S}$ vs x_F at $\sqrt{s} \simeq 17.4$ GeV and $P_T = 2$ GeV for inclusive π^+ (red solid lines) and π^- (blue dashed lines) production in $\mu p^\uparrow \to \pi X$ at COMPASS. Two sets for the quark Sivers and Collins functions have been adopted: SIDIS 1 (left panel) and SIDIS 2 (right panel). The overall statistical uncertainty bands are also shown. Curves have the same meaning as in the previous figure.

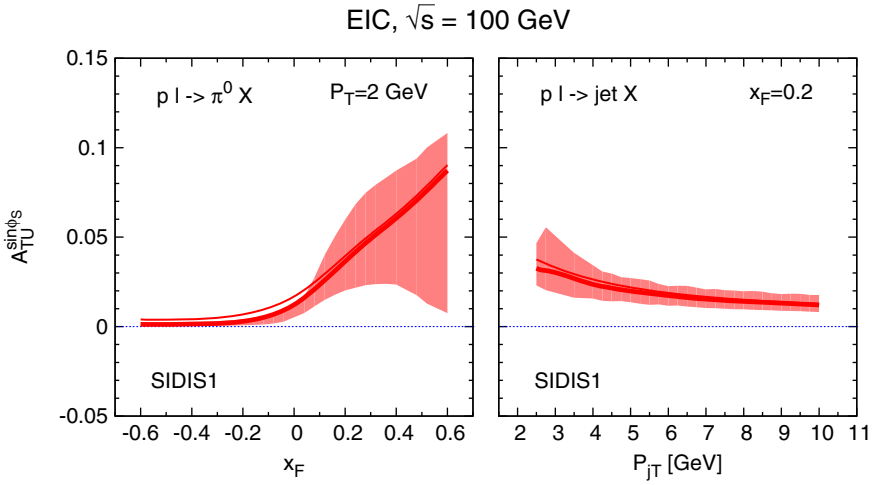

FIG. 12. Theoretical estimates for $A_{TU}^{\sin\phi_S}$ at $\sqrt{s} = 100$ GeV as a function of x_F at $P_T = 2$ GeV for inclusive π^0 production (left panel) and as a function of P_{jT} at $x_F = 0.2$ for inclusive jet production (right panel), adopting the SIDIS 1 set for the quark Sivers and Collins functions. The overall statistical uncertainty bands are also shown. Thick (thin) lines refer to the LO + WW (LO) calculation.

(ii) The corresponding results for π^0 as a function of P_T, not shown, are almost identical to those for inclusive jet production. The same is true for A_N for inclusive jet production as a function of x_F, not shown, almost identical to that for π^0 production.

(iii) As one can see, the WW contribution does not change the LO behavior. This could be expected since both contributions enter with the same structure in the SSA. We then confirm all findings of Ref. [15] concerning the x_F behavior, with the extra important information that at such energies and P_T values the WW piece is the dominant one in the unpolarized cross sections.

(iv) Quite interestingly, the P_T behavior, shown here for the first time, is almost flat and measurable, up to very large-P_T values. This is strongly analogous to what happens in $p^\uparrow p \to \pi^0 X$ as measured by the STAR Collaboration [12], and it would be another very important test of the full approach.

(v) The large error bands at large x_F are due to the still poor knowledge of the Sivers function in the large-x region. Future measurements at JLab could definitely help in this respect.

5. Results from new extractions of the Sivers and Collins functions

At the very last stage of this work, a new extraction of the Sivers functions from the latest SIDIS data has been released [57]. Together with the fit of the Collins and the transversity functions of Ref. [58], they represent the most updated information on the relevant TMDs entering the present analysis. Among the main features of these extractions, we mention the use of the DSS FF set with different Gaussian widths for the unpolarized TMDs, as extracted from SIDIS multiplicities [59], $\langle k_\perp^2 \rangle = 0.57$ GeV^2 and $\langle p_\perp^2 \rangle = 0.12$ GeV^2 [to be compared with those used in SIDIS 1 and SIDIS 2 fits; see Eq. (38)]; the resulting reduced size of the x-dependent part of the valence up and down Sivers distributions; and a more flexible parametrization of the Collins functions, with a more accurate extraction of their transverse momentum dependence. We also notice that for the new fit of the Sivers functions the CTEQ6L parton distribution functions [60] were used.

We then checked the impact of these new parametrizations on the description of HERMES data. The main results are the following: the Collins contribution is practically negligible for the fully inclusive data set and tiny, but slightly improving the description, for the antitagged data category; while still confirming the good agreement with the fully inclusive data, the use of the new Sivers parametrization reduces significantly the discrepancies between the theoretical predictions and the antitagged data for π^+ production (slightly overestimated adopting the SIDIS 1 and SIDIS 2 sets; see Fig. 9, upper panels). In Fig. 13, we present the comparison of these new estimates with the antitagged data, noticing that, even at LO, one gets a clear improvement in the description of π^+ data. No significant differences appear in the unpolarized cross sections, where once again the WW piece is comparable with, or even dominates, the LO contribution.

Analogous features show up also in the predictions for JLab and COMPASS kinematics: almost no differences appear in the unpolarized cross sections, while a reduction in size of the SSAs for π^+ production (roughly a factor of 2 for COMPASS and 3 for JLab with respect to SIDIS 2 estimates) comes out, leading to values for JLab at large x_F of around -10%. For A_N in jet and π^0 production at the EIC, we find similar behaviors as those obtained adopting the SIDIS 1 set (see Fig. 12), with a reduction of our estimates

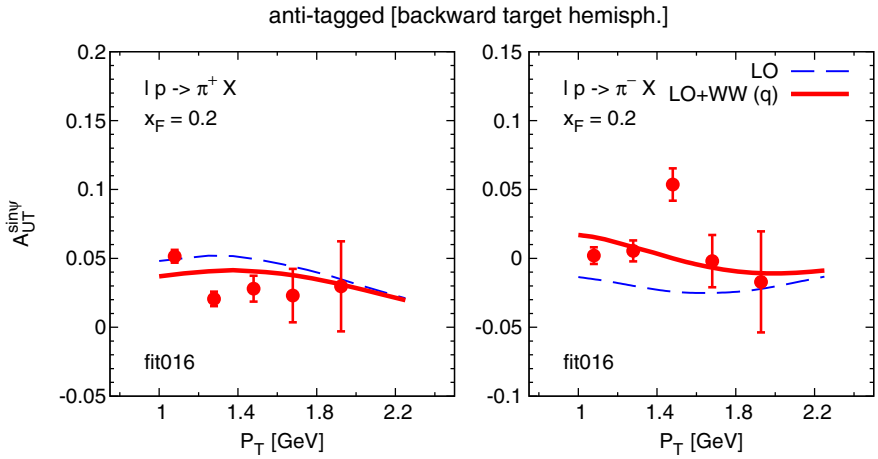

FIG. 13. Theoretical estimates of the Sivers contribution to $A_{UT}^{\sin\psi}$ vs P_T at $\sqrt{s} \simeq 7.25$ GeV and $x_F = 0.2$ for inclusive π^+ (left panel) and π^- (right panel) production in $\ell p^\uparrow \to \pi X$ processes, compared with the antitagged HERMES data [27] and adopting the quark Sivers functions of Ref. [57]. Curves have the following meaning: blue dashed lines for the LO and red solid lines for the LO + WW contributions.

by a factor of 1.5 at fixed x_F vs P_T [that is, $A_N(\text{jet})$ is around 2% at small P_T and 1% at the largest P_T values] and by a factor of about 3 at fixed P_T vs x_F. We have to notice that even if for the P_T dependence this reduction could make the measurement of this asymmetry less feasible, the corresponding uncertainty band still presents a flat behavior, implying a nonvanishing and persisting SSA at large P_T. Concerning the x_F dependence at large-x_F values, one has to take into account the poor knowledge on the Sivers function in the large-x region, heavily affecting also the new extraction.

Some general comments on these results are mandatory:

(i) The new extraction of the Sivers function (the dominant piece) is reasonably under control for HERMES kinematics. On the other hand, some of the assumptions behind it (like the very different Gaussian widths in the unpolarized TMDs), still under current investigation, could have a nonnegligible impact on the predictions at JLab and the EIC (see the above comments on the reduction factors).

(ii) At the present stage, it is then worth keeping and checking also the results obtained adopting the former fits, SIDIS 1 and SIDIS 2, because they are representative of different behaviors in the large-x region, still undetermined, and of different assumptions in their extractions.

(iii) Even if these new extractions seem able to describe HERMES data quite well in a LO approximation, one has to keep in mind that in such a kinematical region the events are strongly dominated by the quasireal photon exchange contribution (see Sec. III A 1).

The fact that the WW piece together with these new extractions gives a very good description of all HERMES data is the most interesting aspect of these results.

IV. CONCLUSIONS

SSAs observed in single-inclusive processes, like those measured in $p^\uparrow p \to hX$, where only one large energy scale is detected, represent a challenging issue in perturbative QCD. Indeed, despite the rich amount of experimental data and their peculiar features, persisting up to the highest available energies, a thorough phenomenological description is so far missing, and many theoretical aspects are still controversial and under debate.

Two approaches are nowadays adopted to describe these SSAs: one based on higher-twist parton correlation functions within a proven collinear factorization framework and one based on transverse momentum-dependent distributions within a phenomenological TMD scheme. Even if not formally proven, this last one enjoys quite considerable phenomenological successes, and it is then worth exploiting it further.

Because of the more complicated nature of SSAs in pp collisions, and the difficulty in understanding their source, a study of SSAs in the theoretical more simple inclusive lepton-nucleon scattering processes, within a TMD scheme, was proposed in Ref. [14] and then analyzed against the available data in Ref. [15]. These processes, moreover, share strong analogies with the SIDIS process for which TMD factorization has been proven. For these reasons, they represent an important testing ground for the understanding of the origin of SSAs.

To assess the validity of the TMD scheme, the single-spin asymmetry A_N, for the $\ell p^\uparrow \to hX$ process, was calculated in a leading-order approximation, adopting the Sivers and the Collins functions as extracted from SIDIS and e^+e^- data. Doing so, a unified TMD factorized approach is adopted, valid for $\ell p \to \ell' hX$ and $\ell p \to hX$ processes, in which, consistently, we obtain information on the TMDs and make predictions for A_N.

In the present analysis, we have extended this strategy, including the contribution of quasireal photon exchange, in the Weizsäcker-Williams approximation, expected to be important when the final lepton is scattered at small angles. To this aim, we have calculated, for the first time, all involved TMD contributions both to the unpolarized and transversely polarized cross sections. We also discussed the role of the WW term in the estimates of the unpolarized cross sections in various experimental setups, showing that it can be extremely important. In particular, at not so large-P_T values (like those explored at HERMES) and at large energies (as those reachable at an EIC), it could be comparable or even dominant with respect to the LO contribution.

More importantly, we have shown how the description of the available SSA data from the HERMES Collaboration is significantly improved when the WW piece is included. Within the present approach, we have also analyzed the antitagged data events, not considered in the previous LO study. Even in this case, our theoretical estimates show a good agreement with the data. It is also worth mentioning that the very few discrepancies in the description of some data sets (namely π^+ antitagged data) seem to disappear when adopting a very recent extraction of the Sivers distributions. This is another successful aspect of the phenomenological consistency of the entire approach. These are, in fact, the main findings of this study.

The role of the gluon Sivers function, which enters through the WW contribution, has been also investigated. Adopting the present knowledge on this TMD, even if with some caution, we have checked that its effect is negligible in most kinematical regions (at least where its extraction is constrained) and does not spoil the agreement with data. Further study would nevertheless be helpful.

Some predictions for ongoing or future experiments have been presented, pointing out the importance of new measurements in testing the overall picture. Notice that in many kinematical configurations the complete (LO+WW) calculation of the SSAs shows a very similar behavior, in size and shape, as for the LO contribution. On the other hand, as extensively discussed, the WW piece changes significantly the expected yields of inclusive particle production.

Among the interesting perspectives of this study, we emphasize that at the EIC, within a TMD scheme, one would expect similar features as those observed in the SSAs for $p^\uparrow p \to \pi X$ processes: the rising of A_N with x_F at fixed P_T, its almost vanishing at negative x_F values, and, somehow surprisingly, a flat behavior of A_N as a function of P_T. The very interesting case of SSAs in inclusive jet production, for which the Collins effect plays no role, has also been discussed, showing features similar to those for the inclusive neutral pion production.

This analysis could definitely be considered a further step toward a deeper understanding of the origin of SSAs in inclusive processes and, more generally, toward a unified TMD picture of these observables. All these findings, although quite encouraging, require further dedicated studies, both on the experimental and the theoretical sides.

ACKNOWLEDGMENTS

We thank M. Schlegel and W. Vogelsang for useful and interesting discussions on the proper use of the Weizsäcker-Williams approximation in this context and M. Anselmino for his careful reading of the manuscript.

APPENDIX: HELICITY FORMALISM

We collect here some details useful for the computation and the understanding of the expressions given in Sec. II B (see Refs. [30,44] for a complete treatment).

We start by recalling the helicity density matrix of a quark q, which can be written in terms of the quark polarization vector components, $\boldsymbol{P}^q = (P^q_x, P^q_y, P^q_z)$, defined in the quark helicity frame, as

$$\rho^{q/p,S}_{\lambda_q,\lambda'_q} = \begin{pmatrix} \rho^q_{++} & \rho^q_{+-} \\ \rho^q_{-+} & \rho^q_{--} \end{pmatrix}_{p,S} = \frac{1}{2}\begin{pmatrix} 1+P^q_z & P^q_x - iP^q_y \\ P^q_x + iP^q_y & 1-P^q_z \end{pmatrix}_{p,S}. \tag{A1}$$

For a gluon (or any spin-1 massless particle), one can define the helicity density matrix as

$$\rho^{g/p,S}_{\lambda_g,\lambda'_g} = \frac{1}{2}\begin{pmatrix} 1+P^g_z & \mathcal{T}^g_1 - i\mathcal{T}^g_2 \\ \mathcal{T}^g_1 + i\mathcal{T}^g_2 & 1-P^g_z \end{pmatrix}_{p,S} = \frac{1}{2}\begin{pmatrix} 1+P^g_{\rm circ} & -P^g_{\rm lin}e^{-2i\phi} \\ -P^g_{\rm lin}e^{2i\phi} & 1-P^g_{\rm circ} \end{pmatrix}_{p,S}. \tag{A2}$$

Equation (A2) refers, in general, to a mixture of circularly and linearly polarized states. $P^g_{\rm circ}$ corresponds to P^g_z, the gluon longitudinal polarization. The off-diagonal elements of Eq. (A2) are related to the linear polarization of the gluons in the (xy) plane at an angle ϕ to the x axis.

Concerning the fragmentation sector, we have for a spinless (or unpolarized) hadron

$$\sum_{\lambda_h} D^{\lambda_h,\lambda_h}_{\lambda_c,\lambda'_c}(z,\boldsymbol{p}_\perp) = D^{h/c}_{\lambda_c,\lambda'_c}(z,\boldsymbol{p}_\perp) = D^{h/c}_{\lambda_c,\lambda'_c}(z,p_\perp)e^{i(\lambda_c-\lambda'_c)\phi^h_c}. \tag{A3}$$

In particular, for the quark fragmentation, we have

$$\hat{D}_{++}(z,\boldsymbol{p}_\perp) = \hat{D}_{--}(z,\boldsymbol{p}_\perp) = D_{h/q}(z,p_\perp) \tag{A4}$$

$$\hat{D}_{+-}(z,\boldsymbol{p}_\perp) = D_{+-}(z,p_\perp)e^{i\phi^h_q} = \frac{i}{2}\Delta^N D_{h/q^\uparrow}(z,p_\perp)e^{i\phi^h_q}, \tag{A5}$$

and for the gluon case,

$$\hat{D}_{++}(z,\boldsymbol{p}_\perp) = \hat{D}_{--}(z,\boldsymbol{p}_\perp) = D_{h/g}(z,p_\perp) \tag{A6}$$

$$\hat{D}_{+-}(z,\boldsymbol{p}_\perp) = D_{+-}(z,p_\perp)e^{2i\phi_g^h} = \frac{1}{2}\Delta^N D_{h/T_1^g}(z,p_\perp)e^{2i\phi_g^h}. \tag{A7}$$

The remaining pieces to be considered are the helicity scattering amplitudes. The transformations (a boost and two rotations) connecting the p–ℓ c.m.frame to the canonical a–γ c.m. frame introduce some nontrivial phases in the helicity amplitudes $\hat{M}_{\lambda_c,\lambda_d;\lambda_a,\lambda_\gamma}$, which are a direct consequence of the nonplanar kinematics.

For massless partons, there are only three independent elementary canonical amplitudes $\hat{M}^0$, corresponding to the $a\gamma \to cd$ processes we are interested in. This allows us to adopt the following notation,

$$\begin{aligned}
\hat{M}_{++;++} &\equiv \hat{M}_1^0 e^{i\varphi_1} \\
\hat{M}_{-+;-+} &\equiv \hat{M}_2^0 e^{i\varphi_2} \\
\hat{M}_{-+;+-} &\equiv \hat{M}_3^0 e^{i\varphi_3},
\end{aligned} \tag{A8}$$

where $\hat{M}_1^0$, $\hat{M}_2^0$, and $\hat{M}_3^0$ are defined as

$$\begin{aligned}
\hat{M}^0_{+,+;+,+} &= \hat{M}^0_{-,-;-,-} \equiv \hat{M}_1^0 \\
\hat{M}^0_{-,+;-,+} &= \hat{M}^0_{+,-;+,-} \equiv \hat{M}_2^0 \\
\hat{M}^0_{-,+;+,-} &= \hat{M}^0_{+,-;-,+} \equiv \hat{M}_3^0,
\end{aligned} \tag{A9}$$

and the phases φ_1, φ_2, and φ_3 can be found in Refs. [30,44]. Notice that the $+$ and $-$ subscripts refer to $(+1/2)$ and $(-1/2)$ helicities for quarks and to $(+1)$ and (-1) helicities for gluons/photons.

[1] U. D'Alesio and F. Murgia, Prog. Part. Nucl. Phys. **61**, 394 (2008).
[2] E. C. Aschenauer, U. D'Alesio, and F. Murgia, Eur. Phys. J. A **52**, 156 (2016).
[3] D. Adams *et al.* (E581 and E704 Collaborations), Phys. Lett. B **261**, 201 (1991).
[4] D. L. Adams *et al.* (FNAL-E704 Collaboration), Phys. Lett. B **264**, 462 (1991).
[5] D. Adams *et al.* (E581 and E704 Collaborations), Phys. Lett. B **276**, 531 (1992).
[6] D. L. Adams *et al.* (E581 Collaboration), Z. Phys. C **56**, 181 (1992).
[7] J. Adams *et al.* (STAR Collaboration), Phys. Rev. Lett. **92**, 171801 (2004).
[8] S. S. Adler *et al.* (PHENIX Collaboration), Phys. Rev. Lett. **95**, 202001 (2005).
[9] J. Lee and F. Videbaek (BRAHMS Collaboration), AIP Conf. Proc. **915**, 533 (2007).
[10] B. Abelev *et al.* (STAR Collaboration), Phys. Rev. Lett. **101**, 222001 (2008).
[11] L. Adamczyk *et al.* (STAR Collaboration), Phys. Rev. D **86**, 051101 (2012).
[12] G. Igo *et al.* (STAR Collaboration), AIP Conf. Proc. **1523**, 188 (2013).
[13] L. Bland *et al.* (AnDY Collaboration), Phys. Lett. B **750**, 660 (2015).
[14] M. Anselmino, M. Boglione, U. D'Alesio, S. Melis, F. Murgia, and A. Prokudin, Phys. Rev. D **81**, 034007 (2010).
[15] M. Anselmino, M. Boglione, U. D'Alesio, S. Melis, F. Murgia, and A. Prokudin, Phys. Rev. D **89**, 114026 (2014).
[16] J. C. Collins, Phys. Lett. B **536**, 43 (2002).
[17] J. C. Collins and A. Metz, Phys. Rev. Lett. **93**, 252001 (2004).
[18] X.-d. Ji, J.-P. Ma, and F. Yuan, Phys. Rev. D **71**, 034005 (2005).
[19] X.-d. Ji, J.-P. Ma, and F. Yuan, Phys. Lett. B **597**, 299 (2004).
[20] A. Bacchetta, D. Boer, M. Diehl, and P. J. Mulders, J. High Energy Phys. 08 (2008) 023.
[21] J. Collins, *Foundations of Perturbative QCD* (Cambridge University Press, Cambridge, England, 2013).
[22] M. G. Echevarria, A. Idilbi, and I. Scimemi, J. High Energy Phys. 07 (2012) 002.
[23] M. G. Echevarria, A. Idilbi, and I. Scimemi, Phys. Rev. D **90**, 014003 (2014).
[24] Y. Koike, Nucl. Phys. **A721**, C364 (2003).
[25] L. Gamberg, Z.-B. Kang, A. Metz, D. Pitonyak, and A. Prokudin, Phys. Rev. D **90**, 074012 (2014).
[26] Z.-B. Kang, A. Metz, J.-W. Qiu, and J. Zhou, Phys. Rev. D **84**, 034046 (2011).
[27] A. Airapetian *et al.* (HERMES Collaboration), Phys. Lett. B **728**, 183 (2014).
[28] P. Hinderer, M. Schlegel, and W. Vogelsang, Phys. Rev. D **92**, 014001 (2015); **93**, 119903(E) (2016).
[29] M. Boglione, U. D'Alesio, and F. Murgia, Phys. Rev. D **77**, 051502 (2008).
[30] M. Anselmino, M. Boglione, U. D'Alesio, E. Leader, S. Melis, and F. Murgia, Phys. Rev. D **73**, 014020 (2006).
[31] D. W. Sivers, Phys. Rev. D **41**, 83 (1990).
[32] D. W. Sivers, Phys. Rev. D **43**, 261 (1991).
[33] A. Bacchetta, U. D'Alesio, M. Diehl, and C. A. Miller, Phys. Rev. D **70**, 117504 (2004).
[34] J. C. Collins, Nucl. Phys. **B396**, 161 (1993).
[35] D. Boer and P. J. Mulders, Phys. Rev. D **57**, 5780 (1998).
[36] D. Boer, Phys. Rev. D **60**, 014012 (1999).
[37] C. F. von Weizsacker, Z. Phys. **88**, 612 (1934).

[38] E. J. Williams, Phys. Rev. **45**, 729 (1934).
[39] S. J. Brodsky, T. Kinoshita, and H. Terazawa, Phys. Rev. D **4**, 1532 (1971).
[40] H. Terazawa, Rev. Mod. Phys. **45**, 615 (1973).
[41] B. A. Kniehl, Phys. Lett. B **254**, 267 (1991).
[42] R. M. Godbole, A. Misra, A. Mukherjee, and V. S. Rawoot, Phys. Rev. D **85**, 094013 (2012).
[43] R. M. Godbole, A. Misra, A. Mukherjee, and V. S. Rawoot, Phys. Rev. D **88**, 014029 (2013).
[44] M. Anselmino, M. Boglione, U. D'Alesio, E. Leader, and F. Murgia, Phys. Rev. D **71**, 014002 (2005).
[45] U. D'Alesio and F. Murgia, Phys. Rev. D **70**, 074009 (2004).
[46] M. Anselmino, M. Boglione, U. D'Alesio, A. Kotzinian, F. Murgia, and A. Prokudin, Phys. Rev. D **71**, 074006 (2005).
[47] M. Gluck, E. Reya, and A. Vogt, Eur. Phys. J. C **5**, 461 (1998).
[48] S. Kretzer, Phys. Rev. D **62**, 054001 (2000).
[49] D. de Florian, R. Sassot, and M. Stratmann, Phys. Rev. D **75**, 114010 (2007).
[50] A. Accardi *et al.*, Eur. Phys. J. A **52**, 268 (2016).
[51] M. Anselmino, M. Boglione, U. D'Alesio, A. Kotzinian, F. Murgia, and A. Prokudin, Phys. Rev. D **72**, 094007 (2005).
[52] M. Anselmino, M. Boglione, U. D'Alesio, A. Kotzinian, F. Murgia, A. Prokudin, and C. Türk, Phys. Rev. D **75**, 054032 (2007).
[53] M. Anselmino, M. Boglione, U. D'Alesio, A. Kotzinian, S. Melis, F. Murgia, and A. Prokudin, Eur. Phys. J. A **39**, 89 (2009).
[54] M. Anselmino, M. Boglione, U. D'Alesio, A. Kotzinian, F. Murgia, A. Prokudin, and S. Melis, Nucl. Phys. B, Proc. Suppl. **191**, 98 (2009).
[55] U. D'Alesio, F. Murgia, and C. Pisano, J. High Energy Phys. 09 (2015) 119.
[56] M. Anselmino, M. Boglione, U. D'Alesio, S. Melis, F. Murgia, and A. Prokudin, Phys. Rev. D **88**, 054023 (2013).
[57] M. Anselmino, M. Boglione, U. D'Alesio, F. Murgia, and A. Prokudin, J. High Energy Phys. 04 (2017) 046.
[58] M. Anselmino, M. Boglione, U. D'Alesio, J. O. Gonzalez Hernandez, S. Melis, F. Murgia, and A. Prokudin, Phys. Rev. D **92**, 114023 (2015).
[59] M. Anselmino, M. Boglione, J. O. Gonzalez Hernandez, S. Melis, and A. Prokudin, J. High Energy Phys. 04 (2014) 005.
[60] J. Pumplin, D. R. Stump, J. Huston, H. L. Lai, P. M. Nadolsky, and W. K. Tung, J. High Energy Phys. 07 (2002) 012.